Size dependence of rutile TiO_2 lattice parameters determined via simultaneous size, strain, and shape modeling

Alexei Y. Kuznetsov,[1] Rogério Machado,[1] Lincoln S. Gomes,[1] Carlos A. Achete,[1] Varghese Swamy,[2,a)] Barry C. Muddle,[2] and Vitali Prakapenka[3]
[1]*Divisão de Metrologia de Materiais—DIMAT, Instituto Nacional de Metrologia, Normalização e Qualidade Industrial, Duque de Caxias, CEP 25250-020 Rio de Janeiro, Brazil*
[2]*Department of Materials Engineering, Monash University, P.O. Box 69M, Victoria 3800, Australia*
[3]*Consortium for Advanced Radiation Sources, University of Chicago, Illinois 60439, USA*

(Received 26 March 2009; accepted 22 April 2009; published online 15 May 2009)

Simultaneous crystal structure, microstructure, and morphology modeling with convolution-based profile fitting of angle-dispersive synchrotron x-ray diffraction data was applied to retrieve the size-dependent lattice changes in nanocrystalline rutile TiO_2. The dominant prismatic crystallite morphology was adequately modeled using the parallelepiped geometry. As with anatase TiO_2, opposing trends of decreasing c and increasing a parameter, as well as lattice expansion with decreasing average crystallite size were observed. A correlation between Ti vacancy abundance and lattice volume increase suggests a possible causative link. © *2009 American Institute of Physics*. [DOI: 10.1063/1.3139078]

The size-dependent property variations in nanocrystalline (nc) materials are typically described as a function of "crystallite sizes" (Ds) obtained from transmission electron microscopy (TEM) or from Scherrer method[1] using powder x-ray diffraction (XRD). While imaging techniques (e.g., TEM) provide direct information on both size and two-dimensional morphology of a limited number of crystallites, the diffraction-methods (Scherrer equation or Rietveld analysis) yield an average crystallite size over a macroscopic sample volume; however, without morphology information. In fact, in diffraction-based investigations of size-dependent lattice changes, it becomes imperative to include morphology information in conjunction with crystal structure and microstructure (crystallite size and microstrain) analysis to achieve accurate size estimates, especially when significantly anisotropic crystallite morphologies (e.g., rodlike or platy shapes) are involved. Further, along with finite crystallite size, morphology and aspect ratios are among the critical parameters governing reactivities at surfaces of materials such as the TiO_2 polymorph anatase.[2]

In this letter, we report size-dependent lattice changes in nc-rutile TiO_2 retrieved via simultaneous modeling of the crystal structure, microstructure, and morphology using angle-dispersive synchrotron XRD data. The current focus on TiO_2 derives from a growing variety of potential applications of nanoscale TiO_2, including in renewable energy and clean environmental technologies,[3] and is driving intense research on the characterization of the finite-scale properties, especially of the most useful TiO_2 polymorphs, anatase, and rutile.

The size-dependent changes in the anatase structure have been widely investigated with most results[4–8] suggesting lattice expansion at small crystallite sizes, as with α-Fe_2O_3 (Ref. 9), CeO_{2-x} (Refs. 10–12), $BaTiO_3$ (Refs. 12 and 13), and $PbTiO_3$ (Ref. 14). However, anatase lattice contraction at small sizes has also been reported.[15] For rutile, lattice expansion with decreasing Scherrer crystallite size was identified from a unit cell volume versus D^{-1} plot[16] using laboratory XRD data. X-ray photoelectron spectroscopy data suggested a covalency enhancement accompanying the lattice expansion.[16]

The crystallite size and morphology variations of the seven nc-rutile samples examined here result from hydrothermal synthesis at different temperatures for 1–3 h.[16–18] TEM revealed elongate crystallites, dominated by prismatic facets with pyramidal terminations (Fig. 1).

Synchrotron XRD measurements were carried out in the Debye–Scherrer geometry at the 13-BMD GSECARS beamline of the Advanced Photon Source (Argonne, USA) with a radiation of wavelength 0.3344 Å. The calibration parameters as well as the source emission profile for the full pattern analysis were obtained using a CeO_2 standard. All the XRD spectra showed broadened peaks characteristic of nc-rutile with a minor amorphous component (Fig. 2).

The XRD spectra were fitted using the convolution-based method[19] implemented in TOPAS-ACADEMIC.[20] The average crystal structure, microstructure, and morphology of the constituent nanocrystals were refined. Two sets of symmetrized spherical harmonics series described the hkl-dependence of the full width at half maximum of Gaussian and Lorentzian components. The convolution of these profile shape functions that vary in 2θ as a function of $1/[\cos(\theta)]$ modeled the size-dependent peak broadening. We also included an hkl-independent strain contribution, modeled with a Voigt function, to the profile shape.

By assuming a certain mean crystallite morphology and size distribution, the "apparent" crystallite sizes (volume-weighted mean column heights) obtained for each hkl reflection can be combined to yield a "true" crystallite size (defined as the cube-root of the crystallite volume) estimate. We assumed a monodispersed, rectangular parallelepiped mean crystallite that closely approximates the morphology seen in the TEM images (Fig. 1). The Scherrer constants linking apparent and true crystallite sizes for the parallelepiped geometry are well known.[21,22]

We used six adjustable parameters—three edge lengths of the parallelepiped (P1, P2, and, P3) and three angles (the Euler's angles ϕ_1, Φ, and ϕ_2) describing the

a)Electronic mail: varghese.swamy@eng.monash.edu.au.

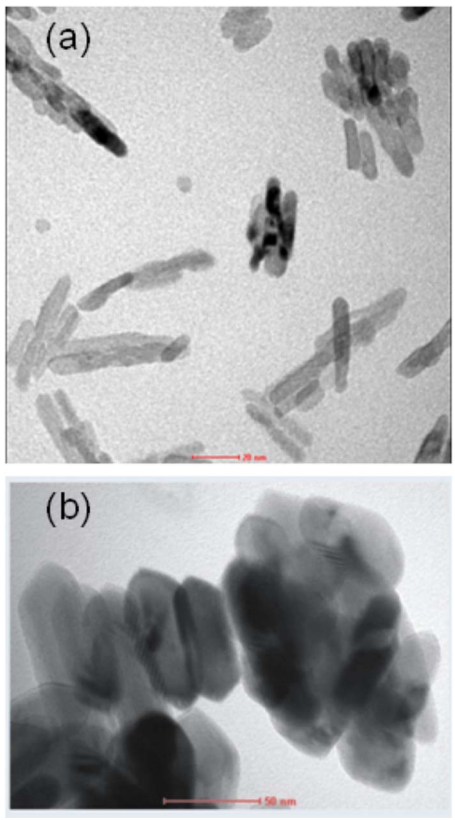

FIG. 1. (Color online) TEM of two hydrothermally synthesized nc-rutile TiO_2 samples. The crystallite morphology is dominated by prismatic facets with pyramidal terminations. The aspect ratios (length-to-breadth) decrease with increasing temperature of synthesis, as exemplified by the samples prepared at 160 °C (a) and 220 °C (b).

crystallographic-morphologic orientation relationship—to translate the apparent sizes to a true crystallite size [Fig. 3(a)]. The parallelepiped edges were chosen as the crystallite (external) coordinate system and the angles ϕ_1, Φ, and ϕ_2 represented the rotation of the crystal coordinate system from the initial orientation in which the crystallographic axes are parallel to those of crystallite coordinate system. The apparent sizes were compared with experimental values by a least-squares procedure that optimized the six model parameters.

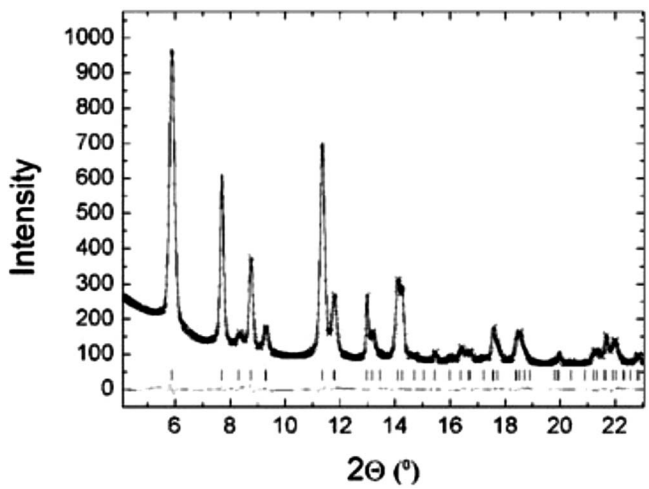

FIG. 2. Experimental (crosses) and convolution-based profile fitted (solid line) XRD patterns of nc-rutile synthesized at 160 °C. The difference between observed and calculated diffraction spectra is plotted at the bottom. The tic marks show the Bragg peak positions of rutile TiO_2.

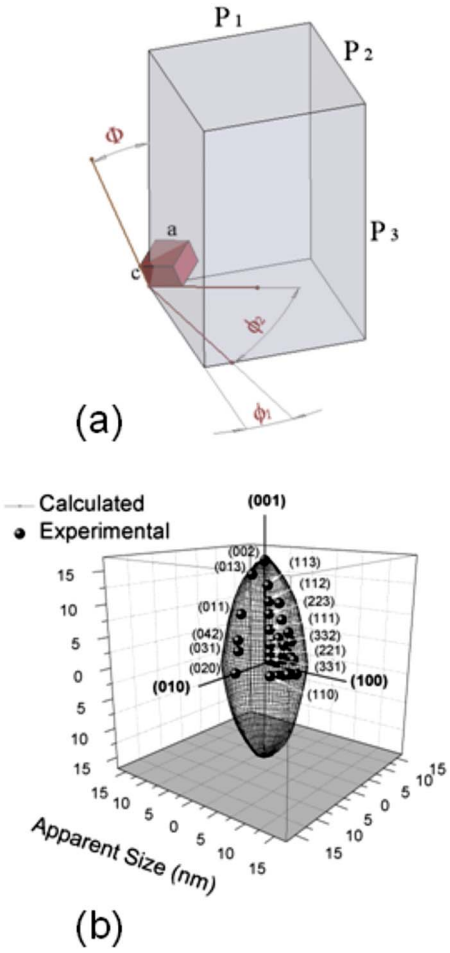

FIG. 3. (Color online) (a) Schematic representation showing the orientational relations between the nc-rutile unit cell and the average prismatic crystallite approximated by a parallelepiped. (b) 3D construction of the apparent crystallite shape produced by a parallelepipedlike crystallite. The apparent crystallite sizes obtained from diffraction peaks (symbols) are plotted as distances from the origin along selected scattering vectors. The 3D mesh represents the theoretical apparent sizes for all possible directions of the scattering vector.

The crystallite shape parameters significantly improved the fit, producing rodlike crystallites with $\Phi \approx 0°$, suggesting that the crystallographic c is collinear with the longest dimension of the crystallites. The final values of ϕ_1 and ϕ_2 fall into two groups: one with $\phi_1+\phi_2 \sim 90°$ and another with $\phi_1+\phi_2 \sim 45°$. This result suggests two dominant orientations for the shorter parallelepiped edges: one along the [110] direction and another along the [020] direction. Figure 3(b) is a three-dimensional (3D) representation of the average crystallite showing apparent shape, as well as theoretical apparent sizes along all possible scattering vectors.

The nc-rutile lattice constants (Fig. 4) show opposite trends as a function of decreasing crystallite size: from bulklike values for the coarsest crystallites, a increases, whereas c decreases leading to an anisotropic size-dependent variation of the unit cell [Fig. 4(a)]. Similar size-dependent variations for nc-anatase unit cell parameters have been reported.[4–6,8]

The antithetic size-dependence of nc-anatase lattice parameters was correlated with Ti vacancy concentration in the structure that is made of distorted TiO_6 octahedra with four shared edges.[8] The presence of Ti vacancies reduces the octahedral edge-sharing and relieves the strong Ti–Ti repulsion,

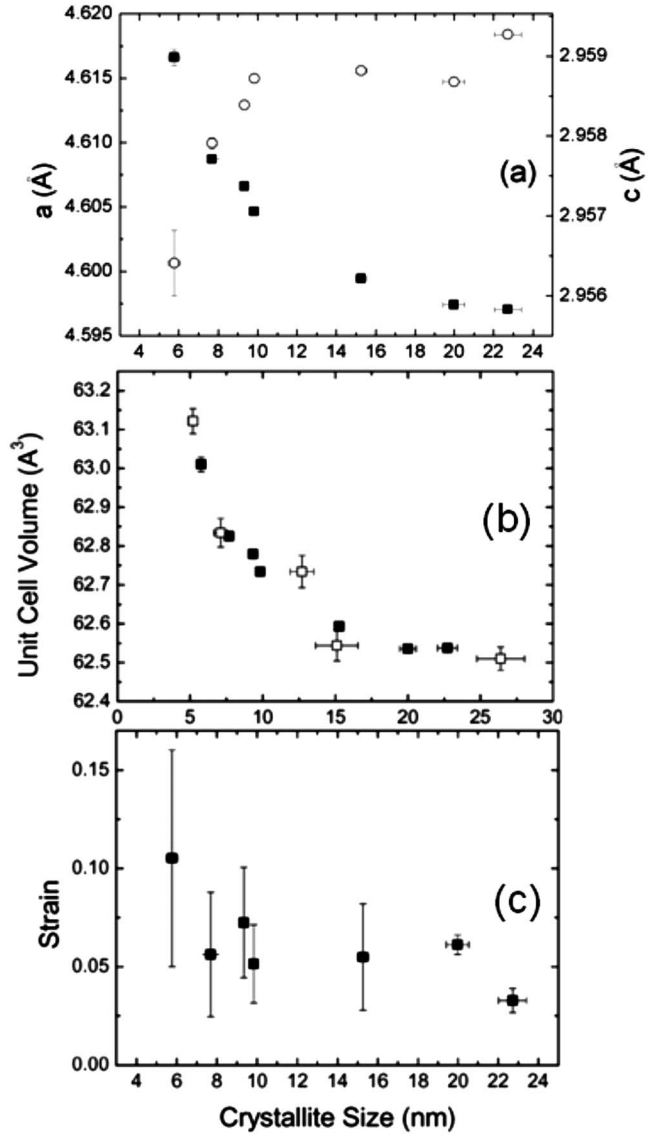

FIG. 4. Size-dependent variations in the unit cell parameters [(a) and (b)] and microstrain (c) of nc-rutile obtained from simultaneous fitting of crystal structure, microstructure, and shape parameters. The open squares represent data from Ref. 16.

leading to regular octahedra and a shortened c parameter and a lengthened a.

Ti^{4+} to Ti^{3+} valence change (cf. CeO_{2-x}, Ref. 12) or oxygen vacancies is unlikely to cause size-dependent lattice changes in anatase or rutile;[6,15,16] Ti vacancies can induce changes, however. Refinement of Ti occupancy, yielding ~90% for coarse crystallites that gradually decrease to <70% for the finest size, improved the fit to the intensity profile significantly. The rutile structure is composed of slightly distorted TiO_6 octahedra that share two opposite parallel edges to form octahedral chains along the c direction. The edge-sharing leads to shorter O–O distances[23] (~2.53 Å) perpendicular to c and relatively longer O–O distances (~2.96 Å) along c. In proportion to the abundance of Ti vacancies, there could be a reduction in the number of shared, edge-shortened TiO_6 octahedra in the structure, and correspondingly, a relaxation in the lengthening along c and shortening perpendicular to it.

An increase in unit cell volume with decreasing crystallite size is seen in Fig. 4(b). The close agreement between our crystallite size versus unit cell volume data and the literature data[16] could be fortuitous. Two counteracting factors typically influence the accuracy of Scherrer estimates based on laboratory XRD data: the inadequate treatment of the instrumental contribution (leading to size underestimation) and the use of a larger Scherrer constant (causing size overestimation). For nanocrystals with extreme morphologies (e.g., rod or plate shapes), the present method will give a truer crystallite size in addition to simultaneously modeling the morphology as well as providing information on cation/anion vacancies, microstrain, etc. The size-dependent microstrains in the nc-rutile lattice obtained in our analysis [Fig. 4(c)] are significantly lower than that seen for nc-anatase,[6] in agreement with the conclusion of an earlier work.[16]

In summary, size-dependent lattice changes of nc-rutile were extracted via simultaneous size, strain, and shape modeling of synchrotron XRD data from a suite of nc samples. In addition to the size-dependent variations in the structure, crystallite size, and microstrain, the size-dependent average crystallite shape variation was also extracted through a morphology modeling invoking simplified parallelepiped geometry.

Financial support from the Australian Research Council and the Australian Synchrotron Research Program is gratefully acknowledged.

[1] H. P. Klug and L. E. Alexander, *X-ray Diffraction Procedures for Polycrystalline and Amorphous Materials* (Wiley, New York, 1974).
[2] H. G. Yang, C. H. Sun, S. Z. Qiao, J. Zou, G. Liu, S. C. Smith, H. M. Cheng, and G. Q. Lu, Nature (London) **453**, 638 (2008).
[3] X. Chen and S. S. Mao, Chem. Rev. (Washington, D.C.) **107**, 2891 (2007).
[4] Y. Li, T. J. White, and S. H. Lim, J. Solid State Chem. **177**, 1372 (2004).
[5] I. Grey, I. Madsen, P. Bordet, N. Wilson, and C. Li, in *Advances in Ecomaterials*, edited by T. White, C. Ferraris, L. Yu, K. Halada, and O. Umezawa (Stallion, Singapore, 2005), Vol. 1, p. 35.
[6] V. Swamy, D. Menzies, B. C. Muddle, A. Kuznetsov, L. S. Dubrovinsky, Q. Dai, and V. Dmitriev, Appl. Phys. Lett. **88**, 243103 (2006).
[7] I. Djerdj and A. M. Tonejc, J. Alloys Compd. **413**, 159 (2006).
[8] I. E. Grey and N. C. Wilson, J. Solid State Chem. **180**, 670 (2007).
[9] D. Schroeer and R. C. Nininger, Phys. Rev. Lett. **19**, 632 (1967).
[10] S. Tsunekawa, R. Sivamohan, S. Ito, A. Kasuya, and T. Fukuda, Nanostruct. Mater. **11**, 141 (1999).
[11] L. Wu, H. J. Wiesmann, A. R. Moodenbaugh, R. F. Klie, Y. Zhu, D. O. Welch, and M. Suenaga, Phys. Rev. B **69**, 125415 (2004).
[12] S. Tsunekawa, K. Ishikawa, Z.-Q. Li, Y. Kawazoe, and A. Kasuya, Phys. Rev. Lett. **85**, 3440 (2000).
[13] S. Tsunekawa, S. Ito, T. Mori, K. Ishikawa, Z.-Q. Li, and Y. Kawazoe, Phys. Rev. B **62**, 3065 (2000).
[14] E. K. Akdogan, C. J. Rawn, W. D. Porter, E. A. Payzant, and A. Safari, J. Appl. Phys. **97**, 084305 (2005).
[15] G. Li, L. Li, J. Boerio-Goates, and B. F. Woodfield, J. Am. Chem. Soc. **127**, 8659 (2005).
[16] G. Li, J. Boerio-Goates, B. F. Woodfield, and L. Li, Appl. Phys. Lett. **85**, 2059 (2004).
[17] V. Swamy, B. C. Muddle, and Q. Dai, Appl. Phys. Lett. **89**, 163118 (2006).
[18] V. Swamy, Phys. Rev. B **77**, 195414 (2008).
[19] A. Kern, A. A. Coelho, and R. W. Cheary, in *Diffraction Analysis of the Microstructure of Materials*, edited by E. J. Mittemeijer and P. Scardi (Springer, New York, 2004), p. 17.
[20] A. A. Coelho, TOPAS-ACADEMIC users manual, http://members.optusnet.com.au/~alancoelho/.
[21] A. R. Stokes and A. J. C. Wilson, Math. Proc. Cambridge Philos. Soc. **38**, 313 (1942).
[22] J. I. Langford and A. J. C. Wilson, J. Appl. Crystallogr. **11**, 102 (1978).
[23] R. C. Evans, *An Introduction to Crystal Chemistry*, 2nd ed. (Cambridge University Press, Cambridge, England, 1964).